Am J Cancer Res 2026;16(10):4603-4620
www.ajcr.us /ISSN:2156-6976/ajcr0174898

Original Article

Novel biomarker APELA inhibits gastric cancer through p21 and epithelial-mesenchymal transition

Chao Hou[1,2], Huichen Xu[3], Lina Yang[1,2], Mingzi Zhang[4], Zhenjiang Yang[1,2], Zhuangzhuang Jiang[5]

[1]Department of Oncology and Hematology, Shenzhen Traditional Chinese Medicine Hospital, Shenzhen 518033, Guangdong, P. R. China; [2]Department of Oncology and Hematology, The Fourth Clinical Medical College of Guangzhou University of Chinese Medicine, Shenzhen 518033, Guangdong, P. R. China; [3]Department of Endocrinology, Shenzhen Hospital (Futian) of Guangzhou University of Chinese Medicine, Shenzhen 518034, Guangdong, P. R. China; [4]Department of Pharmacy, Shenzhen Traditional Chinese Medicine Hospital, Shenzhen 518033, Guangdong, P. R. China; [5]School of Traditional Chinese Pharmacy, China Pharmaceutical University, Nanjing 211198, Jiangsu, P. R. China

Received June 22, 2026; Accepted October 14, 2026; Epub October 15, 2026; Published October 30, 2026

Abstract: Gastric cancer (GC) remains a leading cause of cancer-related mortality worldwide, underscoring the urgent need for novel biomarkers and therapeutic targets. In this study, we analyzed APELA expression in GC using data from The Cancer Genome Atlas (TCGA), the Genotype-Tissue Expression (GTEx) project, and the Gene Expression Omnibus (GEO) database. Kaplan-Meier survival analysis and receiver operating characteristic (ROC) curve analysis were performed to assess its prognostic and diagnostic value, respectively. Gene Ontology (GO), Kyoto Encyclopedia of Genes and Genomes (KEGG), and gene set enrichment analysis (GSEA) were employed to identify associated pathways, while Spearman correlation analysis was used to explore the relationship between Apelin receptor early endogenous ligand (APELA) and epithelial mesenchymal transition (EMT). APELA and the G protein-coupled receptor APLNR (APJ) were further detected in clinical samples by quantitative reverse transcription PCR (qRT-PCR) and immunohistochemistry. Multiple in vitro assays and xenograft models were used to investigate the functional role of APELA. Our results demonstrated that APELA was markedly upregulated in GC tissues, with an area under the curve (AUC) of 0.911 for diagnosis, and that its high expression correlated with improved overall survival. Functional enrichment analyses indicated its involvement in the cell cycle, DNA repair, and EMT. APELA knockdown promoted GC cell proliferation, migration, and invasion, whereas its overexpression exerted the opposite effects. Mechanistically, APELA regulated p21 and inhibited EMT. Collectively, these findings identify APELA as a tumor suppressor in GC that inhibits cell proliferation via p21 and restrains EMT, highlighting its potential as a diagnostic biomarker, prognostic indicator, and therapeutic target for GC.

Keywords: Gastric cancer, APELA, p21, proliferation, epithelial mesenchymal transition

Introduction

Gastric cancer (GC) remains a major global health burden and one of the leading causes of cancer-related mortality [1, 2]. Most patients are diagnosed at advanced stages, when curative intervention is no longer feasible. Current treatment modalities, including surgery, chemotherapy, radiotherapy, and targeted therapy, show limited efficacy against metastatic GC, contributing to a poor overall prognosis [3, 4]. Despite continuous optimization of therapeutic regimens, high rates of recurrence and metastasis remain major clinical challenges. Consequently, novel biomarkers for early diagnosis and effective therapeutic targets are urgently needed to improve the clinical management of GC.

GC exhibits pronounced molecular heterogeneity, and aberrant signaling pathways drive the malignant phenotypes of cancer cells. Apelin receptor early endogenous ligand (APELA, also known as ELABELA) is a secreted peptide hormone that serves as the endogenous ligand for the G protein-coupled receptor APLNR (APJ) [5]. The apelinergic system, comprising APELA, Apelin, and APLNR, regulates multiple physiological processes, including cardiovascular development, fluid balance, and metabolism.

https://doi.org/10.62347/XDKK6578

Under normal conditions, it also contributes to gastrointestinal mucosal protection and tissue repair [6-8]. Unlike the widely distributed Apelin, APELA exhibits restricted tissue expression. To date, its functions have been investigated in only five malignancies, where it primarily modulates tumor cell proliferation [9-11]. However, the role of APELA in GC remains poorly defined. No systematic study has yet elucidated its expression patterns, clinical significance, biological functions, or regulatory mechanisms in GC, leaving a critical research gap.

This study integrated bioinformatics analysis with experimental validation to investigate the function of APELA in GC. Three mainstream public databases were used: The Cancer Genome Atlas (TCGA), the Genotype-Tissue Expression (GTEx) project, and the Gene Expression Omnibus (GEO, https://www.ncbi.nlm.nih.gov/geo/). We first analyzed APELA expression in GC and normal gastric tissues and evaluated its diagnostic and prognostic value. Gene Ontology (GO), Kyoto Encyclopedia of Genes and Genomes (KEGG), and gene set enrichment analysis (GSEA) were performed to identify enriched signaling pathways, and correlation analysis was conducted to explore the association between APELA and epithelial mesenchymal transition (EMT). We further detected the expression of APELA and APLNR in clinical GC specimens via quantitative reverse transcription PCR (qRT-PCR) and immunohistochemistry. A series of in vitro assays were conducted to assess how APELA knockdown and overexpression affect cell proliferation, migration, invasion and EMT. A xenograft mouse model was also established to verify its biological function in vivo.

In conclusion, this study systematically investigated the expression, clinical significance, biological function, and molecular mechanism of APELA in GC. By integrating bioinformatics prediction with experimental validation, we sought to determine whether APELA could serve as a reliable diagnostic biomarker, prognostic indicator, and potential therapeutic target for GC. These findings may provide new theoretical support for targeted therapy in GC.

Materials and methods

Data collection and processing

The mRNA expression data for APELA in tumor samples and matched adjacent non-tumor samples were obtained from TCGA, which also provided the corresponding clinical data of patients with GC [12]. Normal tissue expression data were sourced from the GTEx project. In addition, two datasets, GSE66229 and GSE54129, retrieved from the GEO database, were included as validation cohorts. Transcripts per million reads (TPM) were computed from Level 3 HTSeq-FPKM data of GC patients to facilitate subsequent analysis using R software (version 4.2.1).

Expression analysis of APELA

Samples were stratified according to disease status as either tumor or normal tissue. APELA expression differences between GC and normal samples were visualized using scatter plots and boxplots. Paired samples from TCGA were retained for comparative analysis between tumor specimens and adjacent tissues. Based on the median expression level, GC patients were classified into APELA-low and APELA-high groups.

Diagnostic value analysis

The diagnostic utility of APELA in GC was assessed by receiver operating characteristic (ROC) curve analysis. ROC curves were constructed using the pROC package (version 1.18.0) in the R statistical environment and visualized with the ggplot2 package (version 3.4.3.4) [13]. The area under the curve (AUC) was interpreted as follows: an AUC between 0.5 and 0.7 indicates low diagnostic accuracy, an AUC between 0.7 and 0.9 indicates good accuracy, and an AUC of 0.9 or higher denotes high diagnostic accuracy.

Survival rate analysis

Kaplan-Meier survival analysis with hazard ratios (HR) and log-rank *P*-values was performed using the online KM-Plotter platform (http://kmplot.com/analysis/) [14]. Integrating data from TCGA, GEO (Affymetrix microarrays) and Genome-phenome Archive (GPA), this database covers over 40,000 samples across 21 cancer types, with clinical information for approximately 3.55 million patients including 881 GC cases. We evaluated the association of APELA expression with overall survival (OS), progression-free survival (PFS), and post-progression survival (PPS) in GC using its mRNA microarray dataset.

Differentially expressed genes (DEGs) identification

Differential expression analysis comparing the APELA-High and APELA-Low GC groups was performed using DESeq2 (version 4.0) and Student's t-test. Genes exhibiting an absolute $\log_2$ fold change ($\log_2$FC) > 1 and an adjusted *P*-value < 0.05 were deemed statistically significant. To visualize all DEGs, volcano plots were constructed.

Functional enrichment analysis

We performed GO and KEGG enrichment analyses on the top 152 DEGs ($\log_2$FC > 2.0, adjusted P < 0.05) between APELA-High and APELA-Low groups. The cutoffs were gene number 5-5000, P < 0.05 and false discovery rate (FDR) < 0.25. GSEA was also applied, with significant enrichment defined as |NES| > 1, adjusted P < 0.05 and FDR < 0.25.

Correlation analysis

To evaluate the association of APELA expression with GC proliferation and EMT, the expression levels of key genes implicated in tumor proliferation and EMT were assessed in the APELA-High and APELA-Low GC cohorts. Spearman correlation analysis was performed, and a heatmap depicting single-gene co-expression patterns was generated using an online platform (https://www.xiantaozi.com).

Reagents

MTT and DAPI were obtained from Beyotime (Shanghai, China). ML221 was purchased from MedChemExpress (Shanghai, China).

Cell lines and cell culture

Human GC cell lines (AGS, MKN-28, HGC-27, and MKN-45) and the normal gastric mucosal cell line GES-1 were obtained from Xiamen Immocell Biotechnology Co., Ltd. (Xiamen, China). The cells were cultured in Dulbecco's Modified Eagle Medium (DMEM; Vivacell) supplemented with 10% fetal bovine serum (FBS; Vivacell) and 1% antibiotics (#C0222, Beyotime). All cell lines were maintained at 37°C in a humidified atmosphere containing 5% CO_2.

Cellular transfection

Cells seeded in 6-well plates were transfected with Lipo 6000 (#C0526, Beyotime) in Opti-MEM (#31985-062, Gibco) according to the manufacturer's instructions. APELA-specific shRNA, an APELA overexpression plasmid, and the corresponding control constructs were obtained from Shenzhen Baijing Biotechnology Co., Ltd. (Shenzhen, China). For stable transfection, transfected cells were subsequently selected with puromycin to establish stably transfected cell lines. All experiments were performed in triplicate. The sh-APELA and CMV-APELA sequences are listed in Table S1. The si-p21 sequences are listed in Table S2.

qRT-PCR assay

Total RNA was extracted using TRIzol reagent (#R401-01, Vazyme) according to the manufacturer's instructions. cDNA was synthesized from mRNA using HiScript II RT SuperMix (#R323-01, Vazyme). qPCR analysis was performed using ChamQ SYBR® Green qPCR Mix (#Q341-02, Vazyme), with GAPDH expression used for normalization. For quantitative real-time PCR amplification, each reaction mixture was prepared in a total volume of 20 μL. The amplification mixture consisted of 10 μL of 2 × AceQ qPCR SYBR Green Master Mix, 0.5 μL of forward primer (10 μM), 0.5 μL of reverse primer (10 μM), 4 μL of DEPC-treated water, and 5 μL of cDNA template (diluted to an appropriate concentration). The master mix was first prepared and then dispensed into each well of an 8-tube strip at 15 μL per well, followed by the addition of 5 μL of cDNA sample to each well, reaching a final volume of 20 μL per reaction. After brief centrifugation using a benchtop microcentrifuge, the 8-tube strips were placed into a real-time PCR thermal cycler for amplification. The thermal cycling conditions were as follows: initial denaturation at 95°C for 30 s, followed by 40 cycles of 95°C for 10 s and 60°C for 30 s, with a final extension step [15]. All reactions were performed in triplicate, and relative gene expression was calculated using the $2^{-\Delta\Delta Ct}$ method with GAPDH as the internal control. Primer sequences are listed in Table S3.

Immunohistochemistry

Immunohistochemistry was performed on gastric tissues according to the manufacturer's instructions (#FNAB00485, FineTest). The procedure included rehydration, deparaffinization, antigen retrieval, quenching of endogenous peroxidase activity, and blocking. The tissues were then incubated overnight at 4°C with the

primary antibody (#20341-1-AP, Proteintech, diluted 1:100), followed by incubation with a horseradish peroxidase-conjugated secondary antibody for 30 min at 37°C. APLNR expression was assessed using the Histochemistry Score (H-score) system. Briefly, the H-score was calculated as follows: (1 × the proportion of faintly stained cells) + (2 × the proportion of moderately stained cells) + (3 × the proportion of intensely stained cells) in the area of interest, yielding a final score ranging from 0 to 300. The proportion of cells at each intensity level was determined by counting at least five randomly selected high-power fields per section. The median H-score was used as the cutoff value to dichotomize patients into APLNR-low and APLNR-high expression groups. Any discrepancies were resolved by consensus.

Colony formation assay

To evaluate the effect of APELA on the clonogenic potential of GC cells, transfected cells were seeded in 6-well plates at a density of 1,000 cells per well and incubated for 12 days. The resulting colonies were fixed with 4% paraformaldehyde for 20 min and then stained with 0.1% crystal violet for 15 min. Colonies were counted using ImageJ software.

EdU assay

DNA synthesis rates were assessed using the Click-iT EdU Imaging Kit (#A413, Vazyme) according to the manufacturer's protocol. Briefly, cells were incubated with EdU for 2 h, fixed with 4% paraformaldehyde, permeabilized with 0.3% Triton X-100, and stained with Hoechst 33342. Images were acquired under a fluorescence microscope (Olympus, Japan) [15].

Western blot assay

Cells were rinsed with ice-cold PBS and lysed in RIPA buffer. Protein concentration was measured using a BCA assay (#P00091, Beyotime). Equal aliquots (25 μg) of denatured protein were separated by SDS-PAGE and transferred to PVDF membranes (#GVW2932A, Sigma). The membranes were blocked with 5% skim milk and then incubated with primary antibodies overnight at 4°C. After washing with TBST, the blots were incubated with HRP-conjugated secondary antibodies for 2 h at room temperature. Protein signals were visualized using a Tanon chemiluminescence system and quantified with Image J. The primary and secondary antibodies used are listed in Table S4.

Wound-healing assay

Cells were seeded in 6-well plates and allowed to reach 100% confluence. A linear scratch was created using a pipette tip. The cells were then cultured for an additional 72 h. Wound closure was monitored under an inverted microscope at 0, 24, 48, and 72 h, and the distance between the wound edges was measured.

Migration and invasion assay

For the migration assay, 5×10^4 cells suspended in serum-free medium were seeded into the upper compartment of a 24-well Transwell chamber (8 μm pore size). For the invasion assay, cells were seeded onto inserts pre-coated with Matrigel (#356234, Corning). The lower chamber was filled with complete medium containing 10% fetal bovine serum (FBS) as a chemoattractant. After incubation for 48 h, cells that had not migrated or invaded on the upper side of the membrane were carefully removed with a cotton swab. The incubation time (48 h) was optimized in preliminary experiments, and no saturation of invaded cells was observed in the control groups at this time point. Cells that had successfully traversed to the lower surface were then fixed and stained with 0.1% (w/v) crystal violet solution for 20 min. Migrated or invaded cells were quantified by counting under a standard light microscope (Olympus, Japan).

High-content imaging system analysis

Cells were seeded in a 96-well plate at a density of 5×10^3 cells per well, incubated overnight, and then cultured for an additional 12 h. The plate was subsequently placed into a PerkinElmer Operetta CLS high-content imaging system (PerkinElmer, Waltham, MA, USA) and imaged for 10 h. Briefly, cell motility was monitored using a high-content imaging system with images captured at 10 min intervals over 10 h. Cells were tracked using the built-in tracking algorithm, and only cells that remained within the field of view throughout the recording were included in the analysis. A total of at least 30 cells per group were tracked, and motility parameters including cumulative distance and

average velocity were quantified. These additions ensure that the experimental procedures and quantitative analysis are fully reproducible. Data acquisition and analysis were performed using Harmony 4.1 software.

Design of siRNA and transfection

Gene silencing of p21 was achieved by using small interfering RNA (siRNA). The p21 siRNA and control siRNA were purchased from Genechem (Shanghai China). Transfection was performed using Lipofectamine 6000 transfection reagent (#C0526, Beyotime) according to the manufacturer's instruction. Briefly, AGS-CMV-APELA and MKN-45-CMV-APELA cells were transfected with a well-optimized siRNA mixture containing siRNA duplex, transfection reagent, and Opti-MEM-reduced serum media and then incubated for 24 h at 37°C. The transfection efficiency was confirmed by Western blotting.

Tumor growth assays

BALB/c nude mice (female, 6-8 weeks old, weighing 18-20 g) were obtained from Huachuang Co., Ltd. (Jiangsu, China) and housed at the SPF-grade Laboratory Animal Center of Shenzhen Lingfu Top Biotechnology Co., Ltd. All animal procedures were approved by the Animal Care Committee of Shenzhen Lingfu Top Biotechnology Co., Ltd. (approval No. TOP-IACUC-2024-0288). Animals were assigned to experimental groups using simple randomization, with 5 mice per group (n = 5 per group). Human GC MKN-45 cells stably transfected with CMV-Vector, CMV-APELA, sh-Vector, or sh-APELA (1.0×10^7 cells/100 μL PBS) were injected subcutaneously into the left flank of BALB/c nude mice. Tumor volume and body weight were measured every 3 days. Tumor volume (mm^3) was calculated using the formula: (length × width^2)/2. After approximately 3 weeks, the mice were euthanized, and the volume and weight of the xenograft tissues were measured. Mice were euthanized by cervical dislocation after intraperitoneal injection of pentobarbital sodium (100 mg/kg) for anesthesia. All analyses were performed in a blinded manner, such that the experimenters performing anatomical measurements and data analysis were unaware of the group assignments.

Statistical analysis

Data are expressed as mean ± standard deviation (SD). All experiments were conducted in triplicate. Statistical analyses were performed using GraphPad Prism 10.0 or R software (version 4.2.1). The paired t-test was used to compare H-scores of immunohistochemical staining between GC tissues and matched adjacent non-tumor tissues from the same patients. Two-group comparisons of continuous variables were conducted using Student's t-test (for normally distributed data) or the Mann-Whitney U test (for non-normally distributed data). The χ^2 test or Fisher's exact test was used for categorical variables. For multiple-group comparisons, one-way ANOVA with Tukey's post hoc test was applied. For tumor growth curves, two-way repeated measures ANOVA with Bonferroni's post hoc test was used. Normality was assessed using the Shapiro-Wilk test, and homogeneity of variances was assessed using Levene's test; if these assumptions were violated, the Kruskal-Wallis test was used. For survival analysis, Kaplan-Meier curves were compared using the two-sided log-rank test, and multivariate analysis was performed using Cox proportional hazards models, with censored data handled according to standard methods. A *P*-value < 0.05 was considered statistically significant. Significance levels are indicated as follows: ns, not significant; $^*P < 0.05$; $^{**}P < 0.01$; $^{***}P < 0.001$.

Results

Expression and predictive value of APELA for diagnosis and prognosis

TCGA and GTEx data showed significantly higher APELA expression in GC tissues than in normal tissues (**Figure 1A-C**), which was further verified in paired tumor and paracancerous samples (**Figure 1D**). This trend was also confirmed in the GSE66229 and GSE54129 datasets (**Figure 1E**, **1F**). Consistent with these findings, APELA was upregulated in GC cell lines relative to normal GES-1 cells (**Figure 1G**). Its receptor APLNR was markedly increased in 27 GC specimens compared with adjacent tissues (**Figure 1H**). ROC analysis yielded an AUC of 0.911, indicating strong diagnostic performance of APELA (**Figure 1I**). Kaplan-Meier survival analysis revealed that patients with high

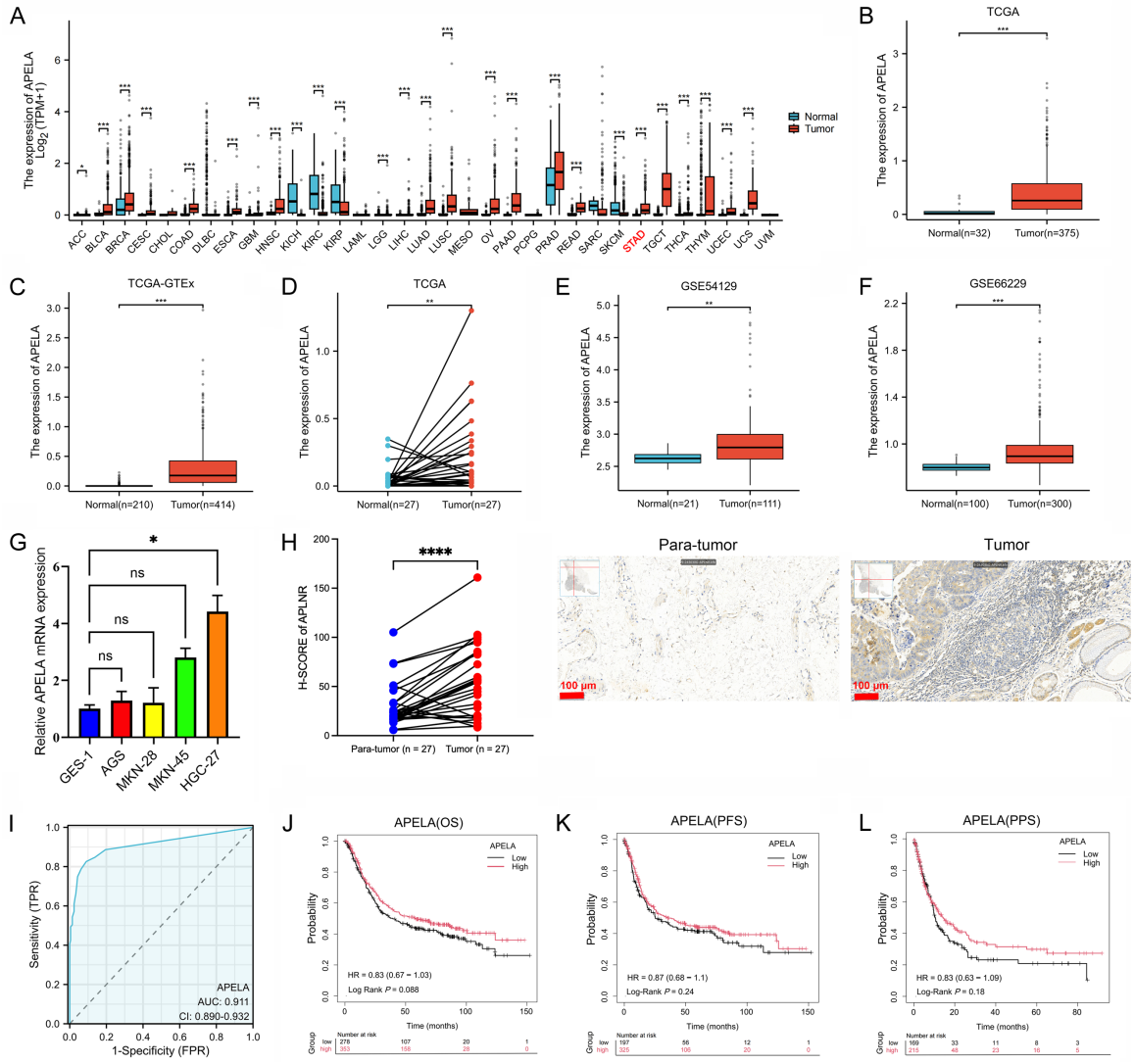


Figure 1. Expression and predictive value of APELA for gastric cancer (GC) diagnosis and prognosis. (A) Expression of APELA in pan-cancer from The Cancer Genome Atlas (TCGA) and Genotype-Tissue Expression (GTEx) databases. (B) Expression levels of APELA in 375 GC tissues and 32 normal tissues from the TCGA database. (C) Expression levels of APELA in 414 GC tissues and 210 normal tissues from TCGA and GTEx databases. (D) Expression levels of APELA in 27 GC tumor tissues and paired para-cancerous tissues from TCGA database. (E, F) Expression of APELA in GSE54129 (E) and GSE66229 (F) datasets. (G) Quantitative reverse transcription PCR (qRT-PCR) analysis of the relative expression of APELA in different GC and GES-1 cells. (H) Immunohistochemical analysis and representative images (magnification 100×) of APLNR in 27 pairs of GC tissue and adjacent non-tumor tissue, Scale bar: 100 μm. (I) Receiver operating characteristic (ROC) curve of APELA in GC. (J) Kaplan-Meier survival curves for overall survival (OS) of GC patients stratified by APELA expression from GSE14210, GSE15459, GSE22377, GSE29272, GSE38749, GSE51105, and GSE62254 datasets. (K, L) Kaplan-Meier survival curves of APELA with progression-free survival (PFS) (K) and post-progression survival (PPS) (L) of GC from GSE14210, GSE15459, GSE22377, and GSE62254 datasets ($^{*}P < 0.05$, $^{**}P < 0.01$, and $^{***}P < 0.001$).

APELA expression had better OS, PFS, and PPS (**Figure 1J-L**). Taken together, these results indicate that APELA is upregulated in GC and may serve as a promising diagnostic and favorable prognostic biomarker.

Relationships between APELA expression and several clinical features in GC

Analysis of the correlations between APELA expression and various clinicopathological

characteristics of GC patients from the TCGA database revealed no significant associations with gender, age, pathologic stage, T stage, N stage, or M stage (**Figure 2A-F**). Kaplan-Meier survival curves further revealed that among GC patients at the T2 or N2 stage, those with higher APELA expression experienced longer OS and PPS than those with lower expression (**Figure 2G-J**). Conversely, among GC patients who received 5-Fu treatment or did not exhibit perforation, higher APELA expression was associated with shorter OS and PFS (**Figure 2K-N**). Moreover, elevated APELA expression in HER2-negative GC patients was associated with improved OS relative to lower expression (**Figure 2O**).

Functional analysis and mutational characterization of APELA

Comparison of 187 APELA-low and 188 APELA-high GC samples identified 8,980 DEGs (8,808 upregulated and 172 downregulated), as illustrated in the volcano plot (**Figure 3A**). The top 1,506 DEGs (log_2 FC > 2.0, adjusted P < 0.05) were subjected to GO and KEGG enrichment analyses (**Figure 3B**, **3C**), linking APELA expression to intermediate filament organization, epidermal development, and pathways such as olfactory transduction and estrogen signaling. GSEA revealed an association between the APELA-low group and EMT, angiogenesis, and adipogenesis (**Figure 3D-F**). In contrast, the APELA-high group showed enrichment in DNA repair, E2F targets, the G2M checkpoint, glycolysis, IL-6/JAK/STAT3, the mitotic spindle, mTORC1, MYC targets, and TNF-α signaling (**Figure 3G-O**), collectively highlighting the biological roles of APELA in GC.

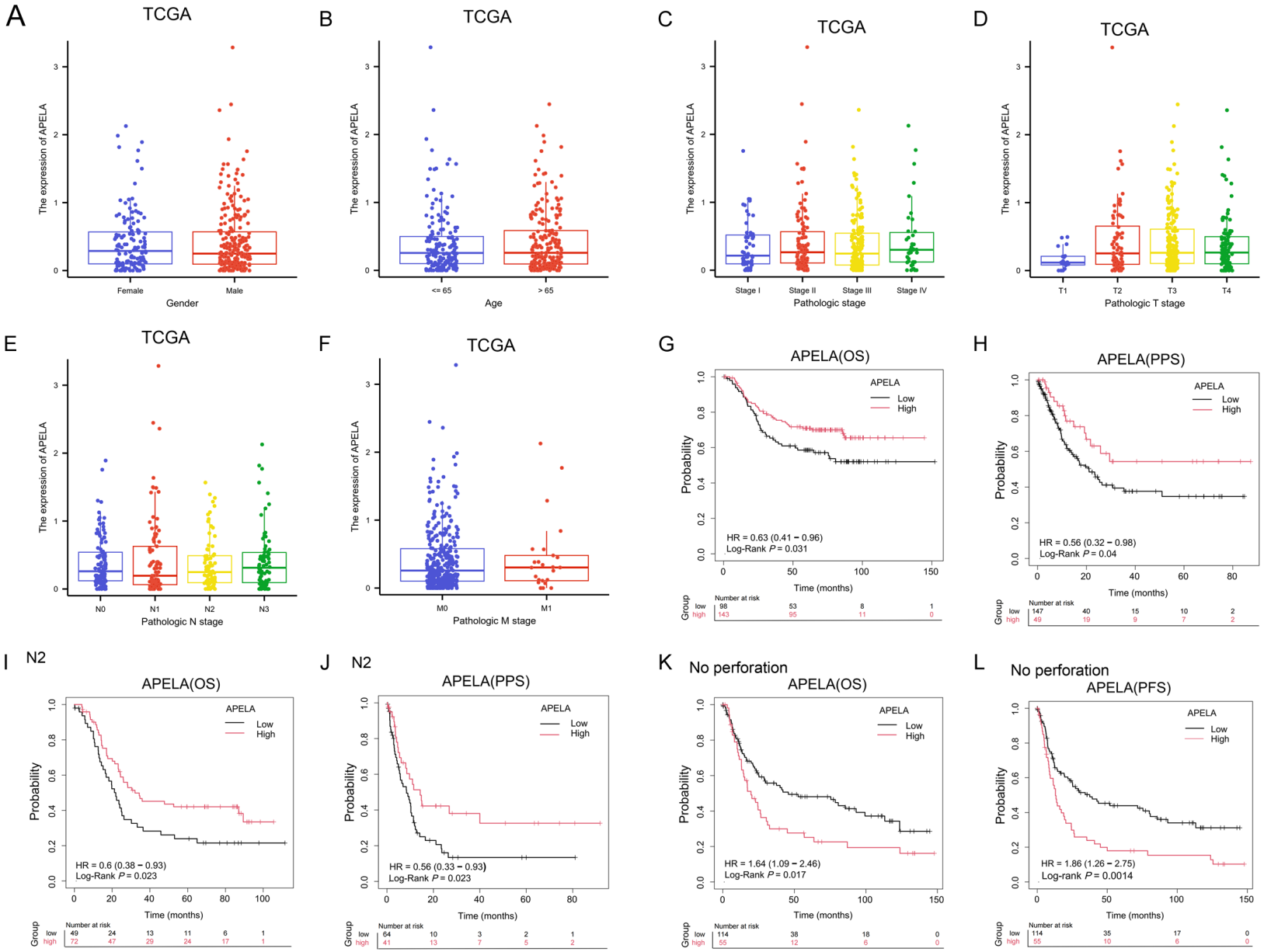
Association with proliferation and EMT

Bioinformatics analysis across three datasets validated the correlation of APELA with proliferation- and EMT-related genes. In proliferation signaling, APELA was correlated with distinct cell cycle genes in the TCGA, GSE66229, and GSE54129 datasets (**Figure 4A-C**). Relative to the APELA-low subgroup, the APELA-high subgroup presented increased NRAS, CDKN2B, and CDKN1C levels but decreased HRAS expression (**Figure 4D-G**), confirming the regulatory role of APELA in GC proliferative networks governing the cell cycle, apoptosis, and differentiation. Moreover, APELA was closely correlated with multiple classic EMT markers across the three independent datasets (**Figure 4H-J**). Consistently, nearly all detected EMT-related genes were significantly upregulated in APELA-high GC samples (**Figure 4K-R**). Collectively, these bioinformatic findings demonstrate that APELA is tightly associated with both tumor proliferation and EMT processes in GC.

APELA attenuates GC proliferation via the p21 signaling axis

Functional assays confirmed that APELA inhibits GC cell proliferation in vitro. We established AGS and MKN-45 cell lines with stable APELA knockdown and overexpression and validated the efficiency of knockdown and overexpression by qRT-PCR (Figure S1). Colony formation and EdU assays revealed that APELA knockdown promoted GC cell proliferation, whereas APELA overexpression suppressed this malignant phenotype (**Figure 5A-C**). Western blot analysis demonstrated that APELA positively regulated the expression of the cell cycle inhibitor p21 (**Figure 5D**, **5E**), indicating that p21 mediates the anti-proliferative effect of APELA. To determine whether p21 mediates the anti-proliferative effect of APELA, we performed p21 knockdown experiments in APELA-overexpressing AGS and MKN-45 cells. Western blot analysis confirmed that transfection with p21-specific siRNA (si-p21) significantly reduced p21 protein expression in both AGS-CMV-APELA and MKN-45-CMV-APELA cells compared with the negative control siRNA (si-Con) (Figure S2A). We then evaluated the effect of p21 knockdown on cell viability using a cell viability assay. As shown in Figure S2B, knockdown of p21 (si-p21) resulted in a significant restoration of cell viability at 48 and 72 hours compared with the si-Con group both in APELA-overexpressing AGS and MKN-45 cells. Collectively, these results demonstrate that p21 knockdown significantly attenuates the anti-proliferative effect of APELA in gastric cancer cells, indicating that p21 is a critical downstream mediator of APELA-induced proliferation inhibition.

Subcutaneous xenograft models were used for in vivo validation. APELA knockdown significantly accelerated tumor growth, with increased tumor volume and weight (**Figure 5F-H**), whereas APELA overexpression markedly restrained tumor formation (**Figure 5J-L**). No significant


A
TCGA
The expression of APELA
Female
Male
Gender
B
TCGA
The expression of APELA
<= 65
> 65
Age
C
TCGA
The expression of APELA
Stage I
Stage II
Stage III
Stage IV
Pathologic stage
D
TCGA
The expression of APELA
T1
T2
T3
T4
Pathologic T stage
E
TCGA
The expression of APELA
N0
N1
N2
N3
Pathologic N stage
F
TCGA
The expression of APELA
M0
M1
Pathologic M stage
G
APELA(OS)
APELA
Low
High
Probability
HR = 0.63 (0.41 − 0.96)
Log-Rank P = 0.031
Time (months)
Group
Number at risk
low 98 53 8 1
high 143 95 11 0
H
APELA(PPS)
APELA
Low
High
Probability
HR = 0.56 (0.32 − 0.98)
Log-Rank P = 0.04
Time (months)
Group
Number at risk
low 147 40 15 10 2
high 49 19 9 7 2
I
N2
APELA(OS)
APELA
Low
High
Probability
HR = 0.6 (0.38 − 0.93)
Log-Rank P = 0.023
Time (months)
Group
Number at risk
low 49 24 13 11 6 1
high 72 47 29 24 17 1
J
N2
APELA(PPS)
APELA
Low
High
Probability
HR = 0.56 (0.33 − 0.93)
Log-Rank P = 0.023
Time (months)
Group
Number at risk
low 64 10 3 2 1
high 41 13 7 5 2
K
No perforation
APELA(OS)
APELA
Low
High
Probability
HR = 1.64 (1.09 − 2.46)
Log-Rank P = 0.017
Time (months)
Group
Number at risk
low 114 38 18 0
high 55 12 6 0
L
No perforation
APELA(PFS)
APELA
Low
High
Probability
HR = 1.86 (1.26 − 2.75)
Log-rank P = 0.0014
Time (months)
Group
Number at risk
low 114 35 17 0
high 55 10 6 0

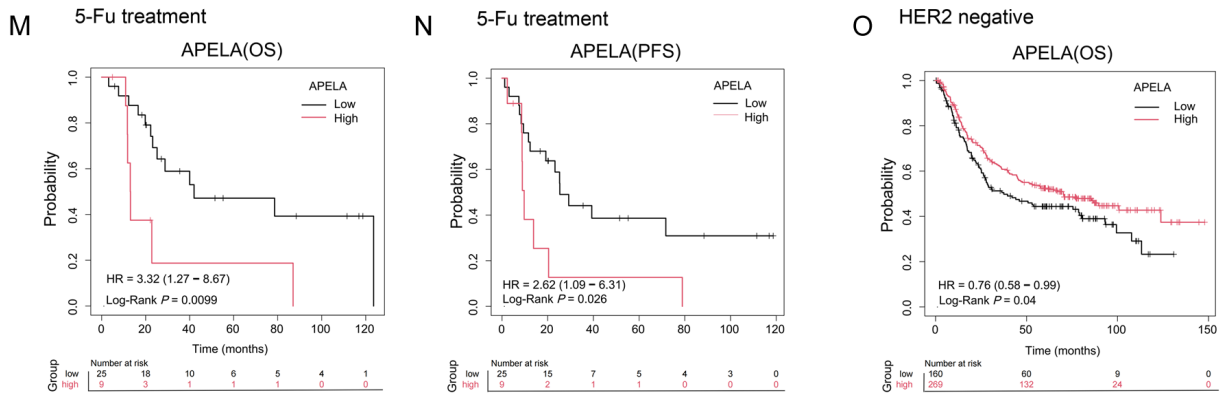
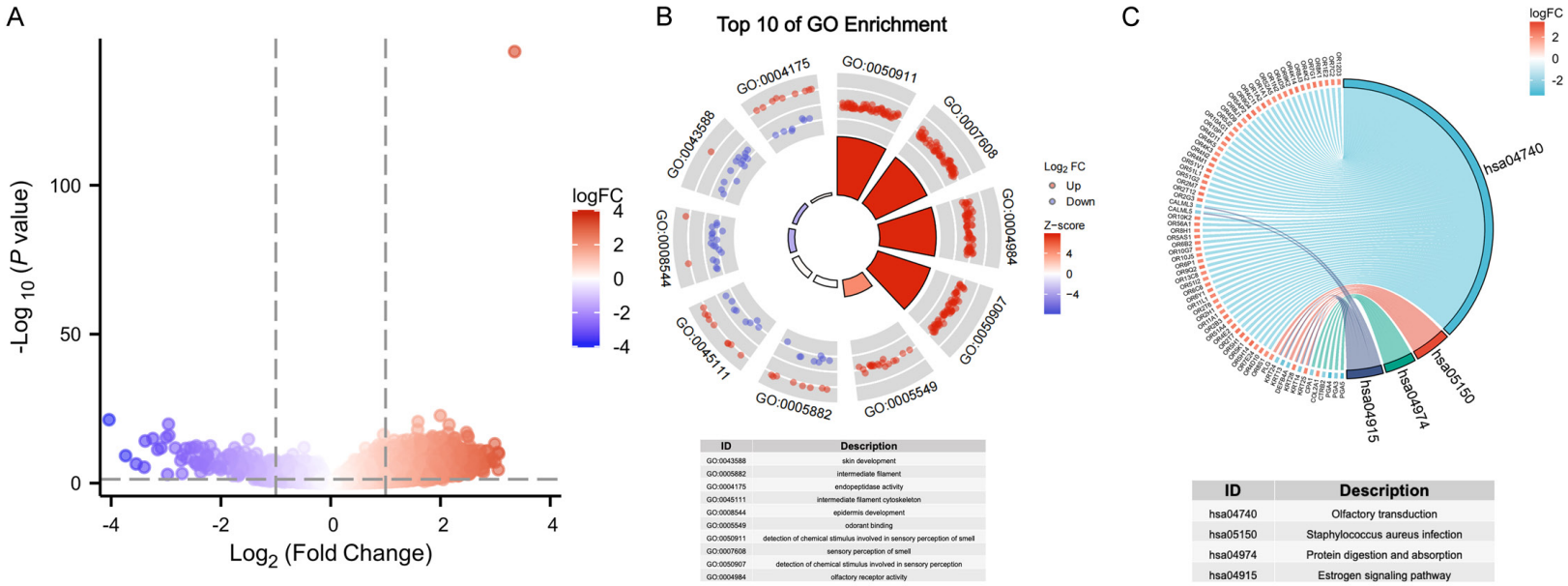


Figure 2. Association of APELA expression with several clinical features. (A-F) Analysis of the correlations between APELA expression levels and various clinicopathological characteristics, including Gender (A), Age (B), Pathologic stage (C), T stage (D), N stage (E), and M stage (F). (G-J) Overall survival (OS) and post-progression survival (PPS) of APELA-high and APELA-low groups were compared using Kaplan-Meier (KM) survival curves in T2 stage (G and H), or N2 stage (I and J) patients. (K-N) OS and progression-free survival (PFS) of APELA-high and APELA-low groups were compared using KM survival curves in patients with no perforation (K and L), or 5-Fu treatment (M and N). (O) OS of APELA-high and APELA-low groups were compared using KM survival curves in HER2-negative patients.



ID	Description
GO:0043588	skin development
GO:0005882	intermediate filament
GO:0004175	endopeptidase activity
GO:0045111	intermediate filament cytoskeleton
GO:0008544	epidermis development
GO:0005549	odorant binding
GO:0050911	detection of chemical stimulus involved in sensory perception of smell
GO:0007608	sensory perception of smell
GO:0050907	detection of chemical stimulus involved in sensory perception
GO:0004984	olfactory receptor activity

ID	Description
hsa04740	Olfactory transduction
hsa05150	Staphylococcus aureus infection
hsa04974	Protein digestion and absorption
hsa04915	Estrogen signaling pathway

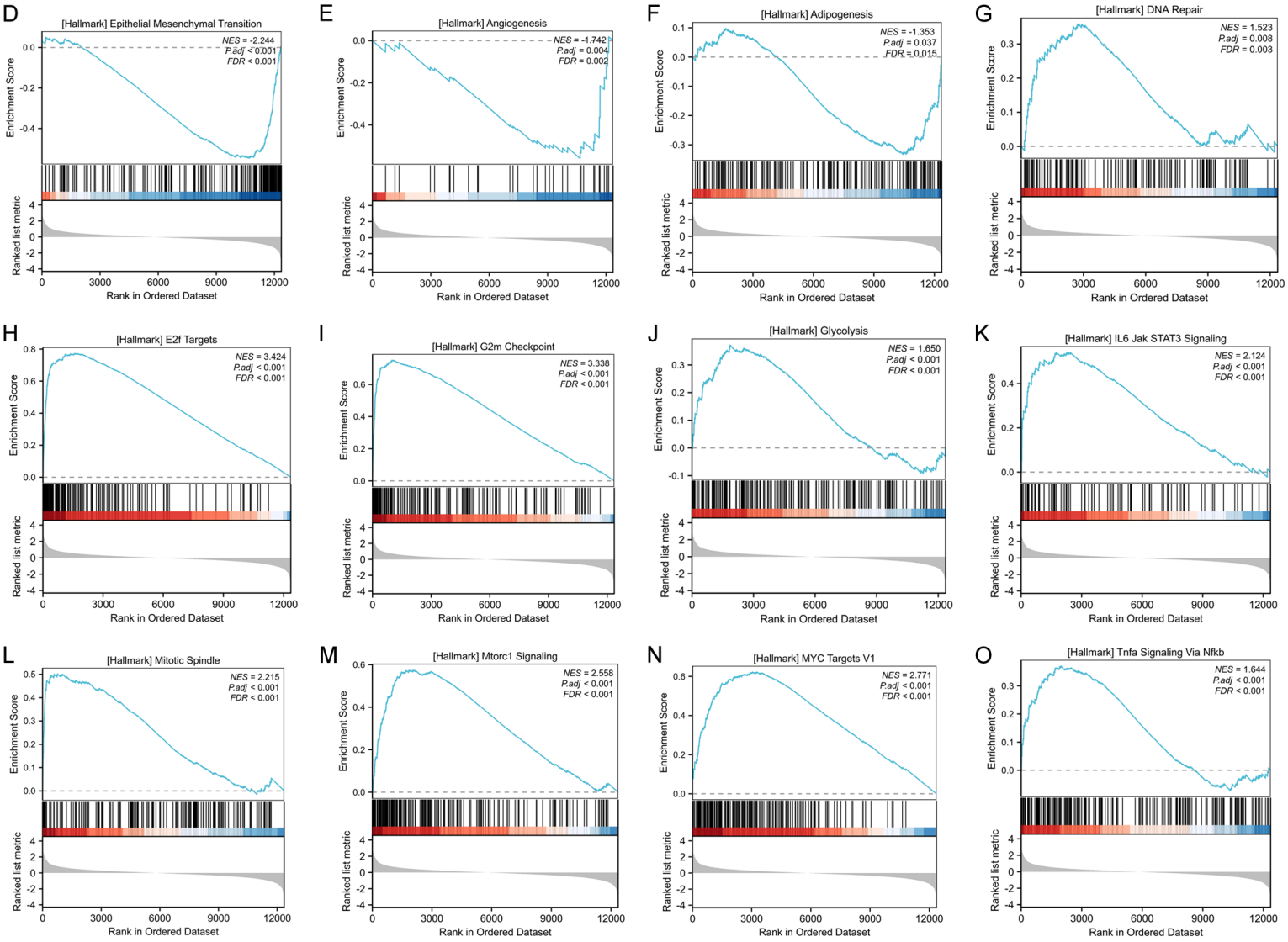


Figure 3. Functional analysis and mutational characterization of APELA. (A) Volcano plot showing differentially expressed genes between 187 APELA-Low and 188 APELA-High samples. (B) The top 10 of gene ontology (GO) enrichment analyses. (C) Kyoto Encyclopedia of Genes and Genomes (KEGG) enrichment analyses. (D-O) Gene set enrichment analysis (GSEA) revealed APELA-related signaling pathways in h.all.v2022.1.Hs.symbols.gmt, including epithelial-mesenchymal transition pathway (D), angiogenesis (E), adipogenesis (F), DNA repair (G), E2F targets (H), G2M checkpoint (I), glycolysis (J), IL-6/JAK/STAT3 signaling (K), mitotic spindle (L), Mtorc1 signaling (M), MYC targets V2 (N), and TNF-α signaling via NF-κB (O).

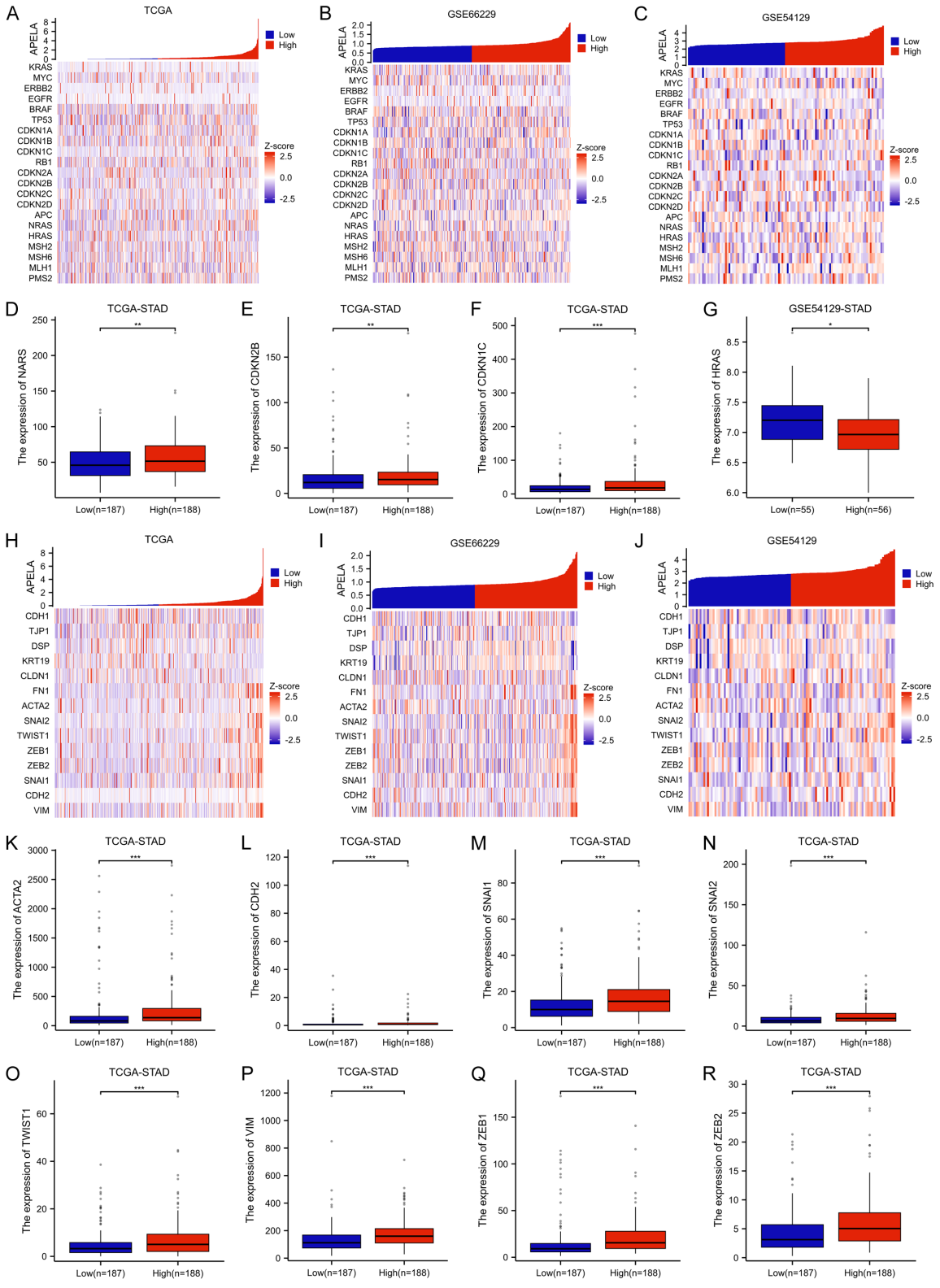


Figure 4. Correlation with proliferation and epithelial-mesenchymal transition (EMT) on APELA. (A-C) The single gene co-expression heatmaps in The Cancer Genome Atlas (TCGA) (A), GSE66229 (B) and GSE54129 (C) datasets, showing the correlation between APELA and the core genes in proliferation pathway network. (D-G) Correlations between the expression levels of NRAS (D), CDKN2B (E), CDKN1C (F), HRAS (G), and APELA are shown in box plots. (H-J) The single gene co-expression heatmaps in TCGA (H), GSE66229 (I) and GSE54129 (J) datasets, showing the correlation between APELA and the core genes in EMT pathway network. (K-R) Relationships between the expressions of ACTA2 (K), CDH2 (L), SNAI1 (M), SNAI2 (N), TWIST1 (O), VIM (P), ZEB1 (Q), ZEB2 (R), and APELA are shown in box plots (*P < 0.05, **P < 0.01, and ***P < 0.001).

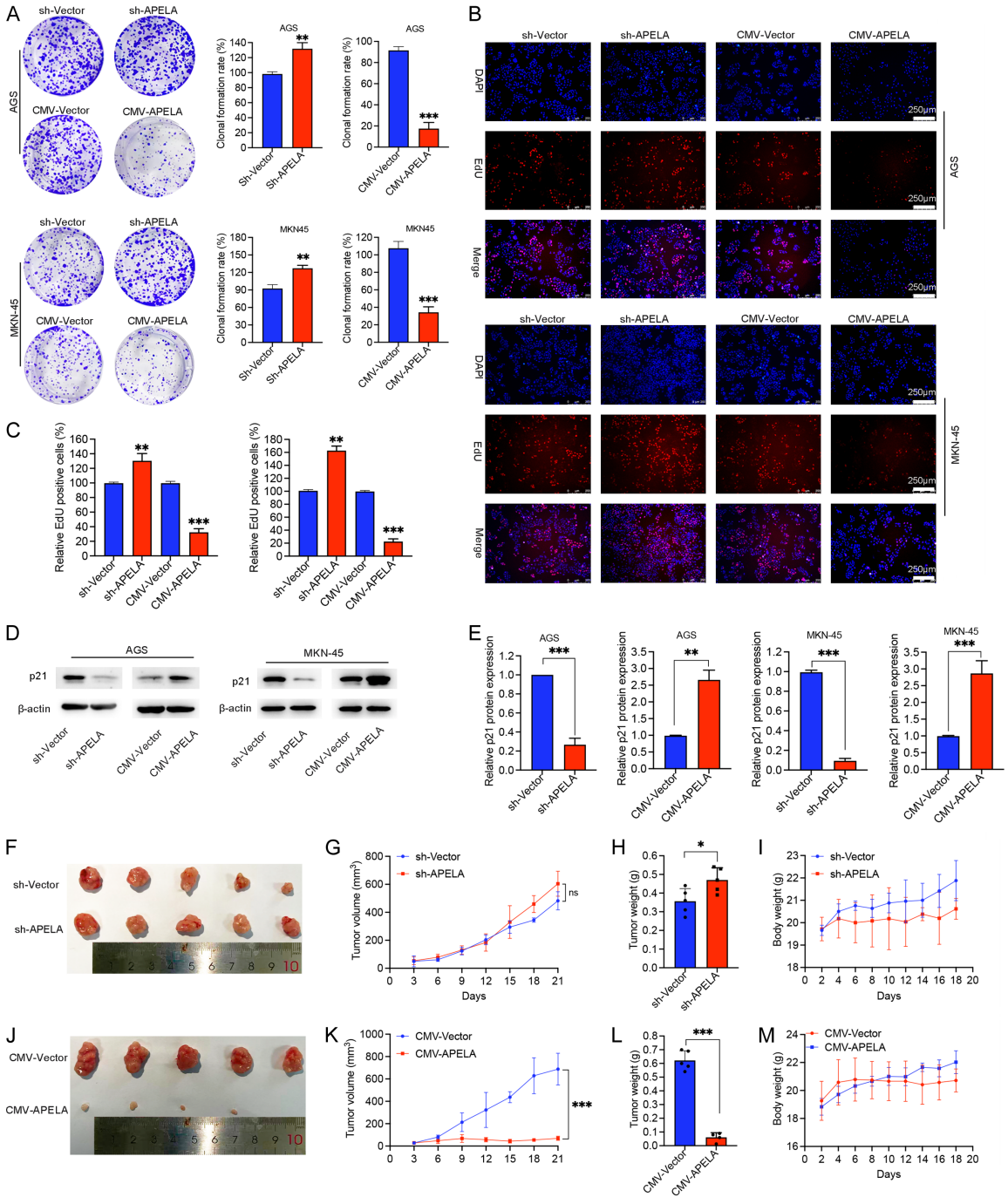


Figure 5. APELA suppresses gastric cancer (GC) cell proliferation by upregulating p21 expression. (A-C) After APELA knockdown or overexpression, colony formation (magnification 1×) (A) and EdU (magnification 100×) (B and C) proliferation assays were performed to assess the proliferative capacity of AGS and MKN-45 cells, Scale bar: 250 μm. (D, E) Western blot analysis and densitometric quantification of p21 protein levels in AGS and MKN-45 cells following APELA knockdown or overexpression. (F-H) Representative images (F), tumor growth curve (G), and tumor weight (H) of xenograft tumor models implanted with MKN-45 cells transfected with sh-Vector or sh-APELA. (J-L) Representative images (J), tumor growth curve (K), and tumor weight (L) of xenograft tumor models implanted with MKN-45 cells transfected with CMV-Vector or CMV-APELA. (I and M) Body weight changes in mice bearing APELA-modified GC xenografts (*P < 0.05, **P < 0.01, ***P < 0.001, and n.s. not significant).

difference in mouse body weight was observed among all groups (**Figure 5I**, **5M**), indicating no systemic side effects induced by APELA intervention. Taken together, these in vitro and in

vivo data verify that APELA serves as a tumor suppressor in GC.

APELA attenuates GC cell migration and invasion by suppressing EMT

Wound healing assays showed that APELA knockdown accelerated migration in AGS and MKN-45 cells, while APELA overexpression hindered wound closure (**Figure 6A**, **6B**). Transwell migration and invasion assays yielded consistent results (**Figure 6C**, **6D**). High-content live-cell tracking further confirmed that APELA silencing enhanced cell motility, and its overexpression exerted the opposite effect (**Figure 6E**, **6F**).

To further investigate the biological role of APELA, we examined its effect on EMT. Western blot analysis revealed that knockdown of APELA (sh-APELA) significantly downregulated the epithelial marker E-Cadherin and upregulated mesenchymal markers, including N-Cadherin, VE-Cadherin, and Vimentin in both AGS and MKN-45 cells. Conversely, overexpression of APELA (CMV-APELA) markedly increased E-Cadherin expression while decreasing the levels of N-Cadherin, VE-Cadherin, Snail, and Vimentin (**Figure 7A-D**). We performed RT-PCR to detect the mRNA expression of E-Cadherin and Vimentin in AGS and MKN-45 cells. As shown in Figure S3, knockdown of APELA (sh-APELA) had no significant effect on the mRNA expression of E-Cadherin and Vimentin in both AGS and MKN-45 cells. In contrast, overexpression of APELA (CMV-APELA) significantly upregulated E-Cadherin mRNA expression in AGS and MKN-45 cells, while markedly downregulating Vimentin mRNA expression in both cell lines. These data suggest that APELA inhibits the EMT process in gastric cancer cells. We next evaluated the effect of APELA on cell proliferation. Cell proliferation assays showed that treatment with the APJ antagonist ML221 dose-dependently reversed the anti-proliferative effect of APELA in both AGS-CMV-APELA and MKN-45-CMV-APELA cells (**Figure 7E**). Consistently, colony formation assays demonstrated that overexpression of APELA significantly suppressed colony formation, whereas the addition of ML221 (10 μM) markedly restored the colony formation rate (**Figure 7F**). These results indicate that the anti-proliferative effect of APELA is mediated through the APJ receptor. To further confirm the role of APJ in APELA-mediated EMT regulation, we treated APELA-overexpressing cells with ML221. Western blot analysis showed that ML221 treatment reversed the APELA-induced upregulation of E-Cadherin and downregulation of N-Cadherin, Vimentin, and Snail. Notably, ML221 also abolished the APELA-induced upregulation of p21 (**Figure 7G**), suggesting that p21 is a downstream effector of APELA/APJ signaling. Finally, we assessed the effect of APELA on cell migration using wound healing assays. Overexpression of APELA significantly inhibited wound closure at 24 h and 48 h in both AGS and MKN-45 cells, while treatment with ML221 (10 μM) significantly accelerated wound closure in APELA-overexpressing cells (Figure S4A, S4B). Collectively, these findings demonstrate that APELA suppresses the proliferation, EMT, and migration of gastric cancer cells, and these effects are dependent on the APJ receptor and involve the upregulation of p21.

Discussion

GC remains a leading cause of cancer-related mortality worldwide, and despite advances in multimodal therapy, the prognosis of patients with advanced or metastatic disease remains poor [2, 16]. There is therefore an urgent need to identify novel molecular mechanisms and therapeutic targets. The apelinergic system, comprising APELA and its receptor APLNR, participates in diverse physiological processes [17]. However, its role in GC pathogenesis remains poorly defined and controversial [18].

In response to this critical requirement, we integrated comprehensive bioinformatics analysis with rigorous experimental validation to define the role of APELA in GC. Although the results demonstrated that APELA mRNA was markedly upregulated in GC, further protein-level validation of APELA is warranted in future studies when appropriate validated antibodies become available. Our results demonstrate that APELA overexpression downregulated the EMT transcription factor Snail and the mesenchymal markers N-cadherin and Vimentin, while upregulating the epithelial marker E-cadherin, thereby reversing the EMT phenotype and inhibiting GC cell migration and invasion. It is noteworthy that the bioinformatic analysis of bulk GC transcriptomes suggested a positive association between APELA expression and EMT-related

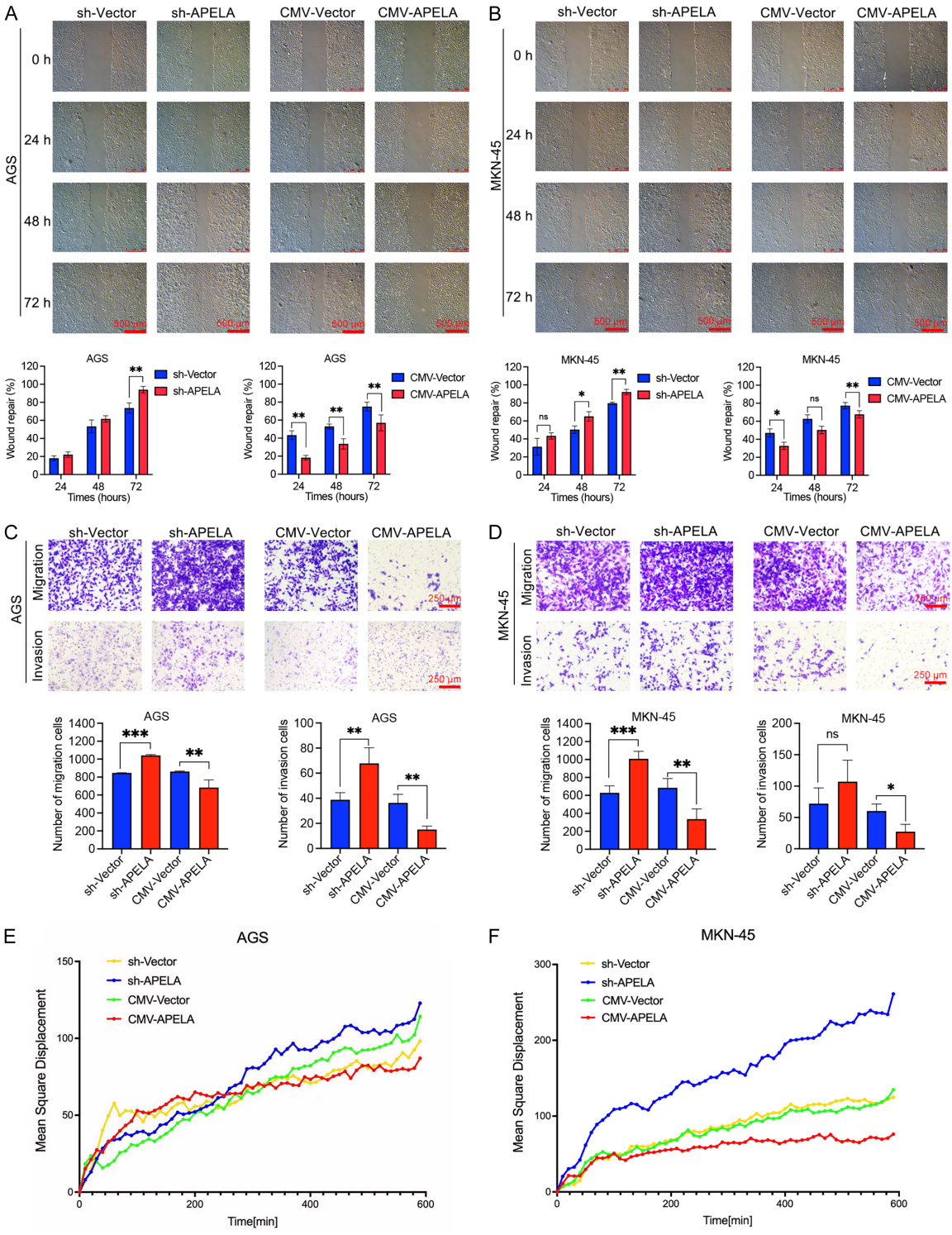


Figure 6. APELA inhibits the migration, and invasion of gastric cancer cells. (A, B) Wound healing (magnification 200×) assays assessed the wound closure rate of AGS (A) and MKN-45 (B) cells transfected with sh-Vector, sh-APELA, CMV-Vector, or CMV-APELA, Scale bar: 500 μm. (C, D) Transwell migration (magnification 100×) and invasion (magnification 100×) assays assessed the migratory and invasive ability of AGS (C) and MKN-45 (D) cells following APELA knockdown or overexpression, Scale bar: 250 μm. (E, F) High-content dynamic tracking assays were conducted to monitor the motility curves of AGS (E) and MKN-45 (F) cells after knockdown or overexpression of APELA (*P < 0.05, **P < 0.01, ***P < 0.001, and n.s. not significant).

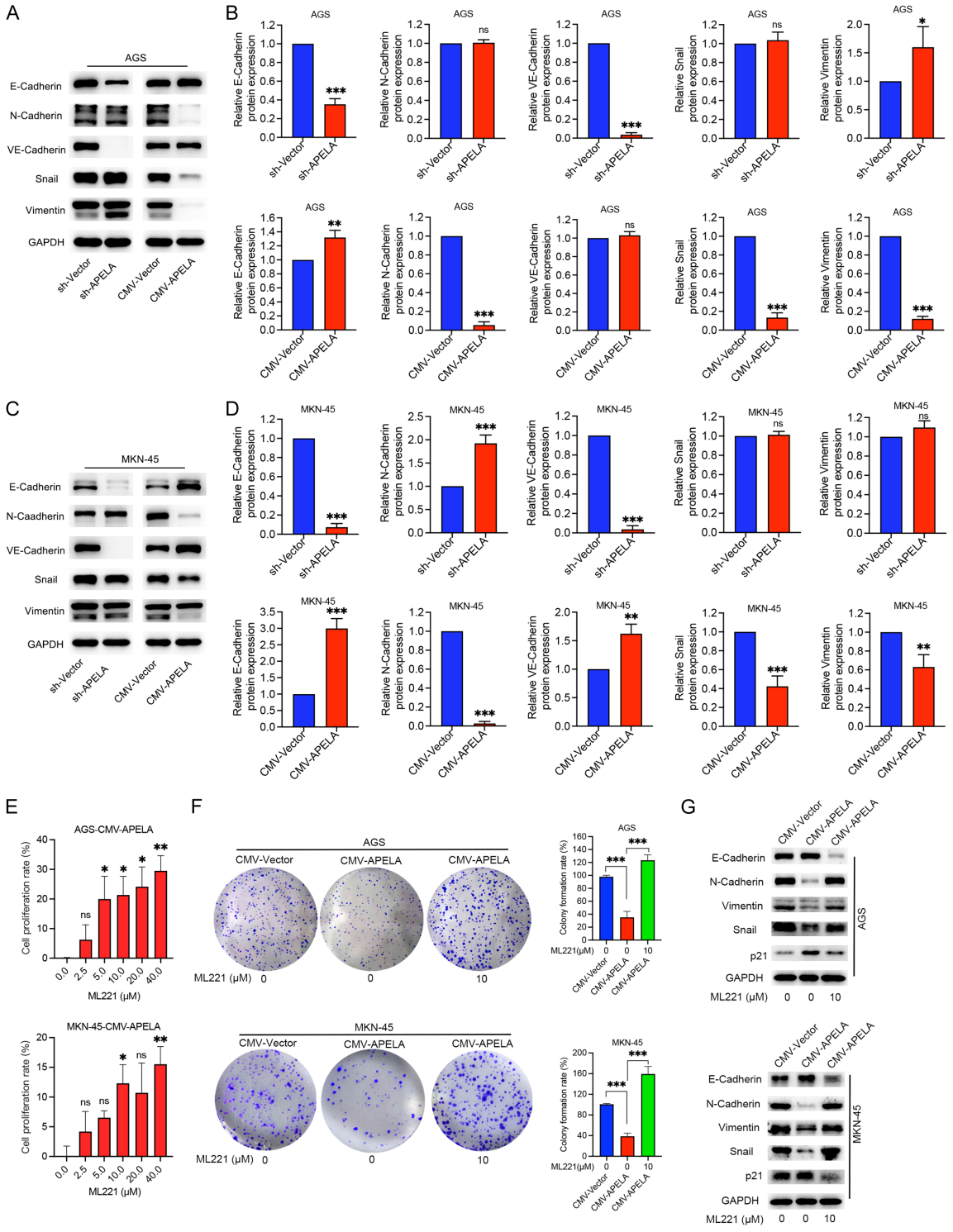


Figure 7. APELA inhibits gastric cancer cell proliferation and epithelial-mesenchymal transition (EMT), which is reversed by ML221. (A, C) Western blot analysis of EMT-related markers (E-Cadherin, N-Cadherin, VE-Cadherin, Snail, and Vimentin) in AGS and MKN-45 cells. (B, D) Relative quantification of the Western blot bands in (A) and (C). (E) ML221 restored the proliferation rate in AGS-CMV-APELA and MKN-45-CMV-APELA cells. (F) Representative images and quantitative analysis of colony formation (magnification 1×) assays. Overexpression of APELA (CMV-APELA) significantly inhibited colony formation in AGS and MKN-45 cells, while the addition of ML221 (10 μM) significantly restored the colony formation rate. (G) Western blot analysis of EMT markers and p21 protein expression in APELA-overexpressing cells treated with ML221 (10 μM). Data are presented as mean ± SD. $^{*}P < 0.05$, $^{**}P < 0.01$, $^{***}P < 0.001$ vs. the control group; ns, not significant.

gene signatures, whereas our functional assays demonstrated that APELA overexpression suppressed EMT and inhibited cell migration and invasion. Several plausible explanations may account for this apparent discrepancy. First, bulk RNA-seq data reflect the average transcriptional profile of all cell types within the tumor mass, including cancer-associated fibroblasts, immune cells, and endothelial cells, all of which are major sources of EMT-related and mesenchymal gene expression. Stromal contamination may therefore mask or reverse tumor cell-intrinsic associations. Second, APELA is a secreted peptide hormone and may exert paracrine effects on neighboring stromal or immune cells, indirectly shaping the EMT-related transcriptomic landscape in a manner not captured by cell-autonomous in vitro assays. Third, bulk transcriptomic correlations do not establish causality, and the EMT gene signature may reflect a general mesenchymal activation state rather than a direct APELA-driven program in tumor cells [19, 20]. Consistent with this, our functional experiments provide direct evidence that APELA overexpression downregulates Snail, N-cadherin, and Vimentin while upregulating E-cadherin in GC cells. Future studies using single-cell RNA sequencing, spatial transcriptomics, or stromal-depleted models will be required to dissect the cell-type-specific and context-dependent effects of APELA on EMT in GC.

In subcutaneous xenograft experiments, APELA overexpression markedly inhibited tumor growth without significant body weight loss, supporting its antitumor efficacy and favorable safety profile. However, this model does not fully recapitulate the complex gastric tumor microenvironment or metastatic progression. Combined with bioinformatic findings linking low APELA expression to angiogenesis pathways, we speculate that APELA may also exert non-cell-autonomous effects. Orthotopic tumor models are therefore needed to further validate its in vivo function. The prognostic implications of APELA appear context dependent. Although high APELA expression is generally associated with better survival, it may exert detrimental effects in specific subgroups, such as patients treated with 5-Fu. This paradox suggests that APELA's role may be modified by external factors such as chemotherapy. Since the APELA/APLNR pathway maintains homeostasis under stress, cytotoxic agents such as 5-Fu could perturb its signaling [5, 9]. For instance, APELA-mediated activation of survival pathways such as PI3K/Akt could enable residual cancer cells to resist genotoxic stress, thereby promoting therapy resistance [21]. GSEA findings provide indirect support for this notion, linking high APELA expression to DNA repair and E2F target pathways associated with chemotherapy response [22]. Thus, functional studies in chemotherapy-treated models are needed to clarify this interaction.

In conclusion, this integrative study identifies APELA as a novel tumor suppressor in GC, with diagnostic potential, favorable prognostic value, and functional roles in inhibiting proliferation via p21 and suppressing EMT. These findings position APELA as a promising candidate for therapeutic intervention. Future studies should focus on elucidating the complete APELA/APLNR signaling axis, validating these mechanisms in orthotopic or metastatic models, and translating these findings into APELA-based diagnostic or therapeutic strategies for clinically relevant patient populations.

Acknowledgements

This work was supported by the Youth Fund of the National Natural Science Foundation of China (82305102), the Sanming Project of Medicine in Shenzhen (SZZYSM202211003), and the Shenzhen High-level Hospital Construction Fund. NewIdea AI (version 2026.2.1) was used solely for language polishing and grammatical revision. No artificial intelligence tool was involved in generating any substantive core content, experimental data, or figures of this manuscript. The authors take full responsibility for the integrity and content of this work.

Disclosure of conflict of interest

None.

Ethics statement

The animal study was reviewed and approved by the Animal Care Committee of Shenzhen Lingfu Top Biotechnology Co., Ltd. (Approval No. TOP-IACUC-2024-0288). The use of human clinical specimens was approved by the Institutional Research Ethics Committees of the Shenzhen Traditional Chinese Medicine Hospital (Approval No. K2026-006-01).

Address correspondence to: Zhuangzhuang Jiang, School of Traditional Chinese Pharmacy, China Pharmaceutical University, 639 Longmian Avenue, Nanjing 211198, Jiangsu, P. R. China. Tel: +86-18851651898; E-mail: 1520250250@cpu.edu.cn; Zhenjiang Yang, Department of Oncology and Hematology, The Fourth Clinical Medical College of Guangzhou University of Chinese Medicine, 1 Fuhua Road, Shenzhen 518033, Guangdong, P. R. China. Tel: +86-13688806551; E-mail: dzjysz@163.com

References

[1] Chen Y, Jia K, Xie Y, Yuan J, Liu D, Jiang L, Peng H, Zhong J, Li J, Zhang X and Shen L. The current landscape of gastric cancer and gastroesophageal junction cancer diagnosis and treatment in China: a comprehensive nationwide cohort analysis. J Hematol Oncol 2025; 18: 42.

[2] Van Laarhoven H. Management of locally advanced gastric cancer. Lancet Oncol 2025; 26: 267-269.

[3] Li W, Zhang P, Cheng M, Wei J, Xu M, Li D, Song S, Liu M, Huang C and Zhu L. XELOX combined with sintilimab and hyperbaric oxygen therapy for advanced or metastatic gastric/gastroesophageal junction adenocarcinoma: study protocol for a prospective, single-arm, phase Ib/II clinical trial. Front Immunol 2026; 16: 1672725.

[4] Albrecht P, Karabati E, Ebert MP and Betge J. Gastric cancer: from biomarkers to functional precision medicine. Trends Mol Med 2025; 31: 1089-1102.

[5] Liet B, Nys N and Siegfried G. Elabela/toddler: new peptide with a promising future in cancer diagnostic and therapy. Biochim Biophys Acta Mol Cell Res 2021; 1868: 119065.

[6] Gemici B, Birsen İ and İzgüt-Uysal VN. The apelin-apela receptor APJ is necessary for formation and healing of ischemia reperfusion-induced gastric ulcer in rats. Peptides 2023; 166: 171027.

[7] Monastero R, Magro D, Venezia M, Pisano C and Balistreri CR. A promising therapeutic peptide and preventive/diagnostic biomarker for age-related diseases: the Elabela/Apela/Toddler peptide. Ageing Res Rev 2023; 91: 102076.

[8] Ho L, Tan SY, Wee S, Wu Y, Tan SJ, Ramakrishna NB, Chng SC, Nama S, Szczerbinska I, Chan YS, Avery S, Tsuneyoshi N, Ng HH, Gunaratne J, Dunn NR and Reversade B. ELABELA is an endogenous growth factor that sustains hESC self-renewal via the PI3K/AKT pathway. Cell Stem Cell 2015; 17: 435-47.

[9] Ganguly D, Cai C, Sims MM, Yang CH, Thomas M, Cheng J, Saad AG and Pfeffer LM. APELA expression in glioma, and its association with patient survival and tumor grade. Pharmaceuticals (Basel) 2019; 12: 45.

[10] Soulet F, Bodineau C, Hooks KB, Descarpentrie J, Alves I, Dubreuil M, Mouchard A, Eugenie M, Hoepffner JL, López JJ, Rosado JA, Soubeyran I, Tomé M, Durán RV, Nikolski M, Villoutreix BO, Evrard S, Siegfried G and Khatib AM. ELA/APELA precursor cleaved by furin displays tumor suppressor function in renal cell carcinoma through mTORC1 activation. JCI Insight 2020; 5: e129070.

[11] Yi Y, Tsai SH, Cheng JC, Wang EY, Anglesio MS, Cochrane DR, Fuller M, Gibb EA, Wei W, Huntsman DG, Karsan A and Hoodless PA. APELA promotes tumour growth and cell migration in ovarian cancer in a p53-dependent manner. Gynecol Oncol 2017; 147: 663-671.

[12] Warde-Farley D, Donaldson SL, Comes O, Zuberi K, Badrawi R, Chao P, Franz M, Grouios C, Kazi F, Lopes CT, Maitland A, Mostafavi S, Montojo J, Shao Q, Wright G, Bader GD and Morris Q. The GeneMANIA prediction server: biological network integration for gene prioritization and predicting gene function. Nucleic Acids Res 2010; 38: W214-20.

[13] Nimbal A, Bahulikar A, Phalgune D and Tambolkar A. Diagnostic and prognostic value of presepsin in sepsis: a prospective observational study. Indian J Crit Care Med 2026; 30: 117-121.

[14] Győrffy B. Integrated analysis of public datasets for the discovery and validation of survival-associated genes in solid tumors. Innovation (Camb) 2024; 5: 100625.

[15] Jiang Z, Ye S, Wu Y, Zhou C, Cao F and Tan N. Cyclopeptide RA-V from Rubia yunnanensis restores activity of Adagrasib against colorectal cancer by reducing the expression of Nrf2. Pharmacol Res 2024; 206: 107252.

[16] Wang FH, Zhang XT, Tang L, Wu Q, Cai MY, Li YF, Qu XJ, Qiu H, Zhang YJ, Ying JE, Zhang J, Sun LY, Lin RB, Wang C, Liu H, Qiu MZ, Guan WL, Rao SX, Ji JF, Xin Y, Sheng WQ, Xu HM, Zhou ZW, Zhou AP, Jin J, Yuan XL, Bi F, Liu TS, Liang H, Zhang YQ, Li GX, Liang J, Liu BR, Shen L, Li J and Xu RH. The Chinese Society of Clinical Oncology (CSCO): Clinical guidelines for the diagnosis and treatment of gastric cancer, 2023. Cancer Commun (Lond) 2024; 44: 127-172.

[17] Wang J, Wang Q, Xu Z, Zhou S, Zhou Y, Yang J, Tong L, Meng Z, Yang M, Zhao W, Yang T, Wang H, Zhang J, Tan R, Wang L, Huang Y, Zhou B, Chen S, Zhang B, Yuan J, Zhao J, Chen AF and Sun K. ELABELA targets mitochondria to modulate heart development. Adv Sci (Weinh) 2026; 13: e06525.

[18] Huang Y, Lin Y, Zhou Q, Liang Y, Lu M, Wu F, Dong Q and Cheng J. U07, a novel oridonin derivative, targets polo-like kinase 4 (PLK4) to

induce ferroptosis in gastric cancer cells. Biochem Pharmacol 2026; 247: 117774.
[19] Hu Y, Bao Q, Huang Y, Wang Y, Zhao X, Nan J, Meng Y, Deng M, Li Y, Zhuang Z, He H, Zu D, Zhong Y, Zhang C, Wang B, Li R, He Y, Wang Q, Liu M, Tainer JA, Shi Y, Cheng X, Jing J and Ye Z. Poly (ADP-ribose) glycohydrolase enforces p21 degradation via dePARylation to promote gastric cancer progression. J Clin Invest 2026; 136: e195538.
[20] Jiang Y, Liao W, Xin Q, Wang R, Lin G, Li J, Yang Z, Yang S, Zhang H, Li X, Peng Q, Zhang Y, Xie W and Xu N. Nuclear and cytoplasmic USP30-AS1 coordinately regulate breast cancer progression through HnRNPF/p21 and EZH2/c-Myc/p21 axes. Genes Dis 2025; 13: 101684.
[21] Respekta N, Pich K, Dawid M, Mlyczyńska E, Kurowska P and Rak A. The apelinergic system: Apelin, ELABELA, and APJ action on cell apoptosis: anti-apoptotic or pro-apoptotic effect? Cells 2022; 12: 150.
[22] Giuntini F, Whitfield JR, Massó-Vallés D and Soucek L. The leading role of MYC in DNA damage response: exploring opportunities for therapeutic inhibition. Front Cell Dev Biol 2026; 13: 1726515.

Table S1. List of sh-APELA and CMV-APELA sequences used

Genes	Primer Sequences
sh-APELA	5'-ACCGGTCCCGCGGACAGAGACCAGTTAATTCAAGAGATTAACTGGTCTCTGTCCGCTTTTTGCTAGC-3'
CMV-APELA	5'-GCTAGCGCCGCCACCATGAGATTTCAGCAATTCCTTTTTGCATTTTTTATTTTTATTATGAGTCTTCTCCTTAT-CAGCGGACAGAGACCAGTTAATTTGACCATGAGAAGAAAACTGCGCAAACACAATTGCCTTCAGAGGAGATGTAT-GCCTCTCCATTCACGAGTACCCTTTCCCTGATGAGGATCC-3'

Table S2. List of si-p21sequences used

Genes	Primer Sequences
si-p21	5'-GUGGACAGCGAGCAGCUGAdTdT-3'

Table S3. List of primer sequences used

Genes	Primer Sequences
APELA	Forward: 5'-ACACCCAGCCACACAAAAGA-3'
	Reverse: 5'-CTCCCTATTGTGCGAAGCCA-3'
E-Cadherin	Forward: 5'-ATTTTTCCCTCGACACCCGAT-3'
	Reverse: 5'-TCCCAGGCGTAGACCAAGA-3'
Vimentin	Forward: 5'-AGTCCACTGAGTACCGGAGAC-3'
	Reverse: 5'-CATTTCACGCATCTGGCGTTC-3'
GAPDH	Forward: 5'-GGTTGTCTCCTGCGACTTCA-3'
	Reverse: 5'-TGGTCCAGGGTTTCTTACTCC-3'

Table S4. List of antibodies used

Antibodies	Company	Catalog#	Host	Dilution
APLNR	Proteintech	20341-1-AP	Rabbit	1:1000
p21	Proteintech	10355-1-AP	Rabbit	1:1000
E-Cadherin	Proteintech	20874-1-AP	Rabbit	1:1000
N-Cadherin	Proteintech	22018-1-AP	Rabbit	1:1000
VE-Cadherin	Proteintech	27956-1-AP	Rabbit	1:1000
Snail	Proteintech	13099-1-AP	Rabbit	1:1000
Vimentin	Proteintech	10366-1-AP	Rabbit	1:1000
GAPDH	Proteintech	10494-1-AP	Rabbit	1:1000
β-actin	Proteintech	66009-1-Ig	Mouse	1:1000
Anti-Rabbit	Proteintech	SA00001-1		1:5000
Anti-Mouse	Proteintech	SA00001-2		1:5000

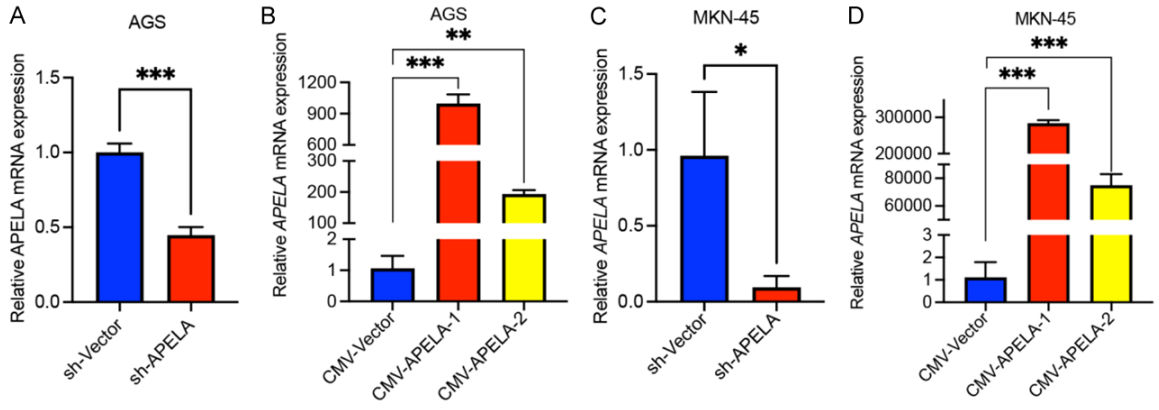


Figure S1. Validation of APELA knockdown and overexpression efficiency in GC cell lines. (A, C). Relative APELA mRNA expression in AGS (A) and MKN-45 (C) cells transduced with sh-APELA or sh-Vector, as determined by qRT-PCR. (B, D). Relative APELA mRNA expression in AGS (B) and MKN-45 (D) cells transduced with CMV-APELA-1, CMV-APELA-2, or CMV-Vector, as determined by qRT-PCR. Data are presented as mean ± SD. *P < 0.05, ***P < 0.001.

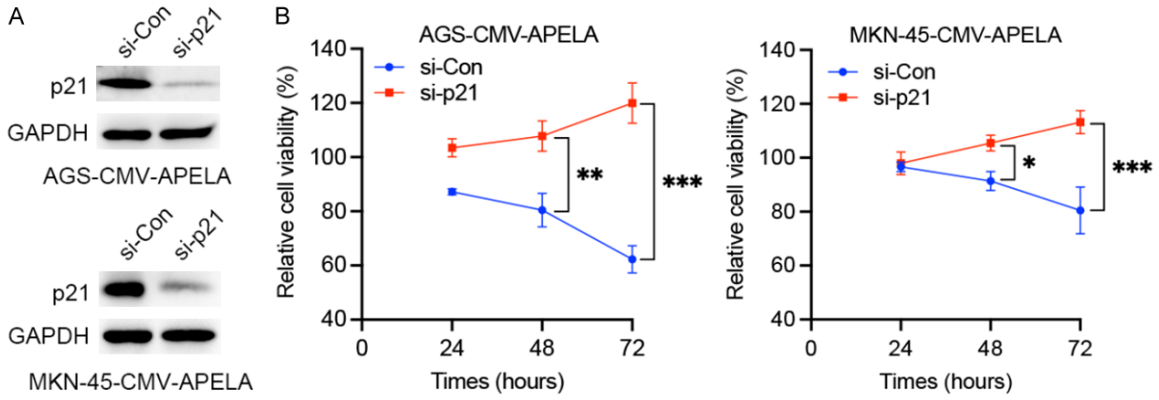


Figure S2. Knockdown of p21 reverses the anti-proliferative effect of APELA in gastric cancer cells. A. Western blot analysis confirming the successful knockdown of p21 protein expression by specific siRNA (si-p21) in AGS-CMV-APELA and MKN-45-CMV-APELA cells. GAPDH was used as a loading control. B. Cell viability assays showing that p21 knockdown (si-p21) significantly restored cell viability at 24, 48, and 72 h in APELA-overexpressing AGS and MKN-45 cells, reversing the anti-proliferative effect of APELA. Blue circles represent the control group (si-Con), and red squares represent the p21 knockdown group (si-p21). Data are presented as mean ± SD. **P < 0.01, ***P < 0.001 vs. si-Con group.

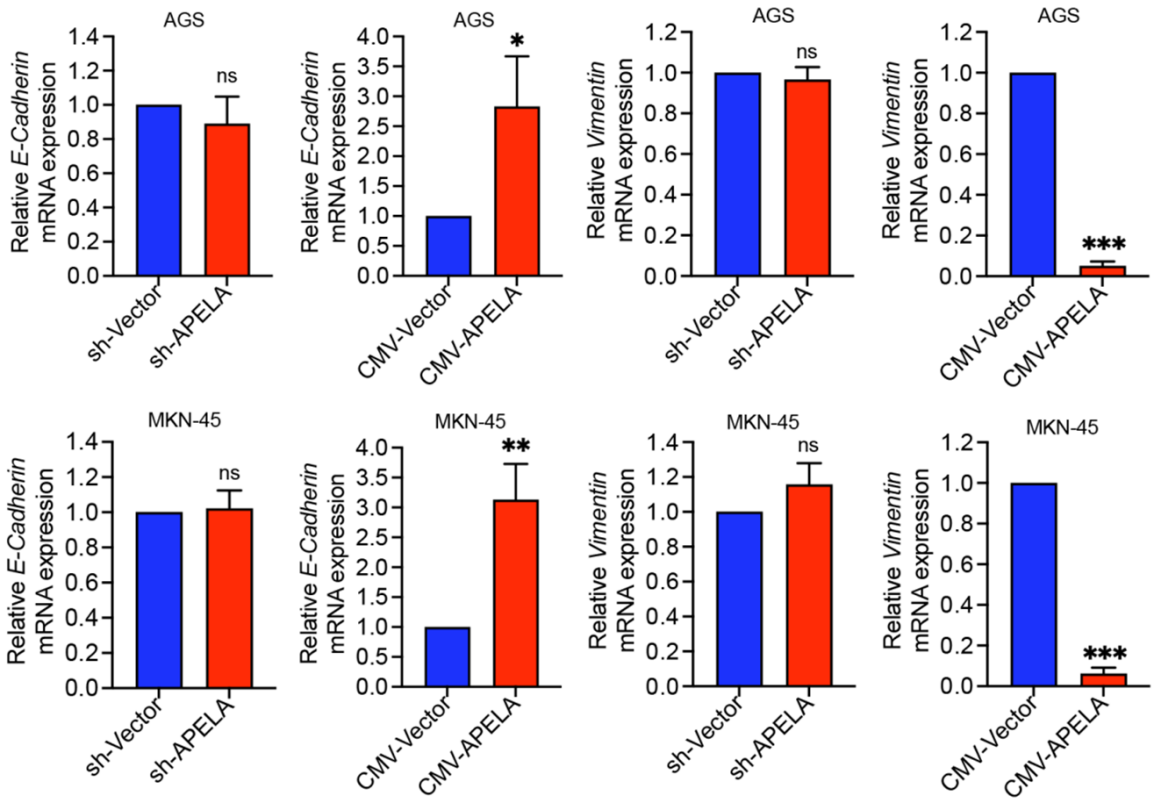


Figure S3. Relative mRNA expression levels of E-Cadherin and Vimentin were detected by RT-qPCR in AGS and MKN-45 cells. Data are presented as mean ± SD. *P < 0.05, **P < 0.01, ***P < 0.001 vs. the control group (sh-Vector or CMV-Vector); ns, not significant.

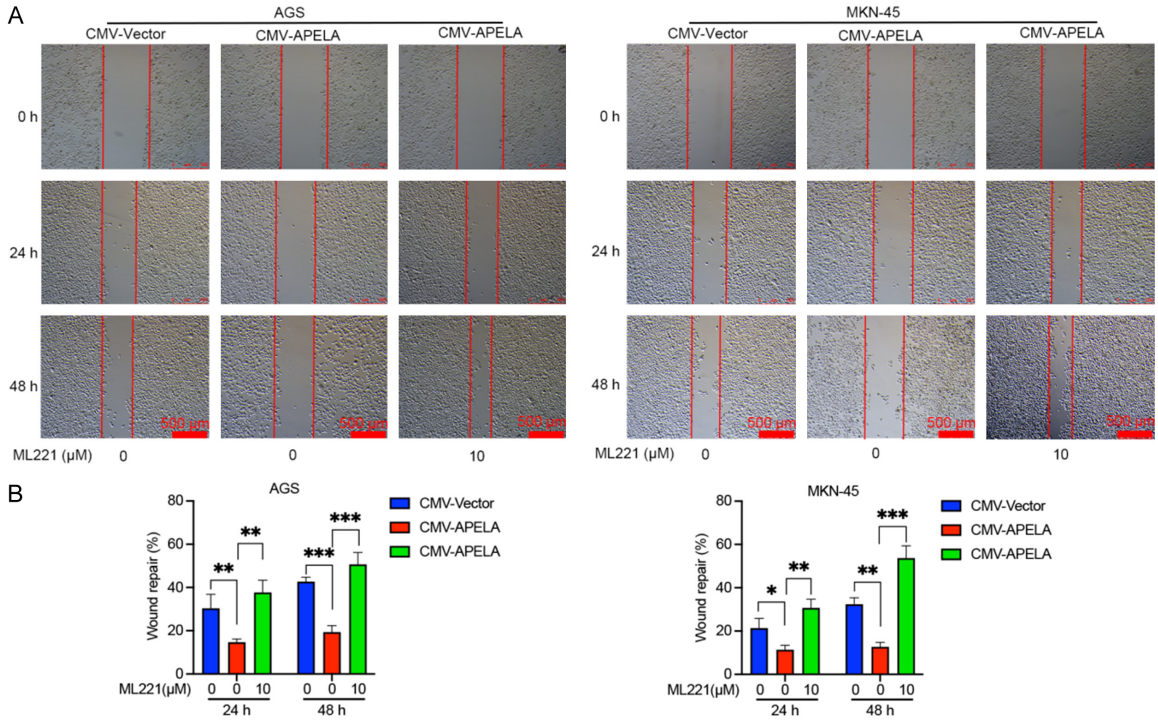


Figure S4. ML221 reverses the inhibitory effect of APELA on gastric cancer cell migration. A. Representative images of the wound healing (magnification 200×) assay. Red dashed lines indicate the wound edges. Scale bar, 500 μm. B. Quantitative analysis of the wound healing rate. Data are presented as mean ± SD. *P < 0.05, **P < 0.01 vs. CMV-Vector group; ***P < 0.001 vs. CMV-APELA.